THE JOURNAL OF BIOLOGICAL CHEMISTRY VOL. 286, NO. 27, pp. 23959–23966, July 8, 2011

Hexafluoroisopropanol Induces Amyloid Fibrils of Islet Amyloid Polypeptide by Enhancing Both Hydrophobic and Electrostatic Interactions*[S]

Received for publication, January 31, 2011, and in revised form, April 28, 2011 Published, JBC Papers in Press, May 12, 2011, DOI 10.1074/jbc.M111.226688

Kotaro Yanagi[1], **Mizue Ashizaki**[1], **Hisashi Yagi, Kazumasa Sakurai, Young-Ho Lee, and Yuji Goto**[2]

From the Institute for Protein Research, Osaka University, Yamadaoka 3-2, Suita, Osaka 565-0871, Japan

Although amyloid fibrils deposit with various proteins, the comprehensive mechanism by which they form remains unclear. We studied the formation of fibrils of human islet amyloid polypeptide associated with type II diabetes in the presence of various concentrations of 1,1,1,3,3,3-hexafluoroisopropanol (HFIP) under acidic and neutral pH conditions using CD, amyloid-specific thioflavin T fluorescence, fluorescence imaging with thioflavin T, and atomic force microscopy. At low pH, the formation of fibrils was promoted by HFIP with an optimum at 5% (v/v). At neutral pH in the absence of HFIP, significant amounts of amorphous aggregates formed in addition to the fibrils. The addition of HFIP suppressed the formation of amorphous aggregates, leading to a predominance of fibrils with an optimum effect at 25% (v/v). Under both conditions, higher concentrations of HFIP dissolved the fibrils and stabilized the α-helical structure. The results indicate that fibrils and amorphous aggregates are different types of precipitates formed by exclusion from water-HFIP mixtures. The exclusion occurs through the combined effects of hydrophobic interactions and electrostatic interactions, both of which are strengthened by low concentrations of HFIP, and a subtle balance between the two types of interactions determines whether the fibrils or amorphous aggregates dominate. We suggest a general view of how the structure of precipitates varies dramatically from single crystals to amyloid fibrils and amorphous aggregates.

Amyloid fibrils play an important role in a range of diseases, including Alzheimer's disease, dialysis-related amyloidosis, and type II diabetes mellitus (1–4). In addition, various proteins and peptides not related to amyloidosis form similar fibrillar deposits *in vitro* (5). In several cases, the fibrillar deposits are functional (6, 7). Although the biological impact of amyloid fibrils is tremendous, we still do not have a general view of why and how the fibrils form. On the other hand, we have increasing evidence suggesting the underlying mechanism of fibril formation. 1) First, fibril formation is coupled with the denaturation of proteins (8–10), suggesting that it is a property of unfolded or non-native proteins. 2) Hydrophobicity is a dominant factor determining the amyloidogenicity of proteins. Because the cross-β structure with a hydrogen bond network is essential for the fibrils (11), the propensity of side chains as well as the main chains to form hydrogen bonds is also important. 3) Alcohols, particularly 2,2,2-trifluoroethanol (TFE)[3] (12) or 1,1,1,3,3,3-hexafluoroisopropanol (HFIP) (13), are useful as cosolvents to induce fibrils. Interestingly, amyloidogenicity is enhanced only at moderate concentrations of alcohols. This is also true of detergents like SDS, for which a concentration close to the critical micelle concentration (CMC) is effective (13–15). We suggested that the effects of SDS can be interpreted similarly to those of alcohols (13). 4) One of the most important aspects of amyloidogenicity not focused on so far is that fibrils are common to shorter peptides but rare for proteins of more than 200 amino acids. As far as we know, no case was reported where an entire region of a molecule of more than 20,000 formed fibrils (16, 17). On the other hand, short fragments tend to exhibit stronger amyloidogenicity than the original proteins (18). For an example, medin, a 50-residue-long peptide produced from lactadherin, a 364-residue glycoprotein, is a main component of aortic medical amyloid (19). It is worth noting that various peptide hormones easily form fibrils. Short amyloidogenic peptides form microcrystals useful for obtaining structural insights into amyloid fibrils (11, 20, 21). Taking these findings together, one should consider the formation of amyloid fibrils with respect to the solubility of proteins and peptides in a denatured state. Vendruscolo and co-workers (22, 23) studied this issue by simulating the competition between folding and aggregation and the solubility of proteins. At the same time, one should consider the difference between amyloid fibrils and amorphous aggregates. To address these issues, it would be useful to examine the effects of alcohols.

The effects of alcohols on proteins and peptides have been investigated extensively, including the destruction of the native conformation, the induction of α-helices, and the dissolution of peptide aggregates (24). These effects can be explained by the polarity of the solvent (24). In solvents of low polarity, the hydrophobic interactions stabilizing the native structure or

* This work was supported by grants-in-aid from the Japanese Ministry of Education, Culture, Sports, Science, and Technology and by the Japan Society for the Promotion of Science Research Fellowships for Young Scientists (to H. Y.).

[S] The on-line version of this article (available at http://www.jbc.org) contains supplemental Figs. S1–S4 and Movies S1–S3.

[1] Both authors contributed equally to this work.

[2] To whom correspondence should be addressed: Institute for Protein Research, Osaka University, Yamadaoka 3-2, Suita, Osaka 565-0871, Japan. Tel.: 81-6-6879-8614; Fax: 81-6-6879-8616; E-mail: ygoto@protein.osaka-u.ac.jp.

[3] The abbreviations used are: TFE, 2,2,2-trifluoroethanol; HFIP, 1,1,1,3,3,3-hexafluoroisopropanol; CMC, critical micelle concentration; hIAPP, human islet amyloid polypeptide; ThT, thioflavin T; AFM, atomic force microscopy; TEM, transmission electron microscopy; TIRFM, total internal reflection fluorescence microscopy.

peptide aggregates are weakened, and simultaneously local hydrogen bonds are strengthened, resulting in denaturation and the stabilization of extended α-helical structures. Among various alcohols, TFE and HFIP are often used because of their marked potential (25). This efficiency is linked with the propensity of these alcohols to form dynamic clusters via hydrophobic interactions (26). The effects of detergents such as SDS can be interpreted in a similar way, in which the formation of micelles is important to understand their effects (13).

To examine the effects of alcohols on amyloidogenic proteins in detail, we used human islet amyloid polypeptide (hIAPP, also known as amylin) with a high propensity to form amorphous aggregates as well as amyloid fibrils. hIAPP is a 37-residue peptide hormone with an amidated C terminus and an intramolecular disulfide bond between Cys-2 and Cys-7 (supplemental Fig. S1*A*). Amyloid fibrils of hIAPP deposit near pancreatic β-cells of type II diabetes, with their presence strongly correlating with a loss of β-cell mass and decreased pancreatic function (27–32). Soluble hIAPP adopts a predominantly random coil structure, suggesting that it is intrinsically unfolded. Recent structural studies point toward its interaction with membranes (33, 34) and an α-helical structure on membranes (12, 34, 35), suggesting the helical intermediate to be on the pathway to the formation of fibrils.

In this study, we examined the formation of fibrils by hIAPP in the presence of various concentrations of HFIP using CD, thioflavin T (ThT) fluorescence, atomic force microscopy (AFM), and total internal reflection fluorescence microscopy (TIRFM) (36–39). We revealed that moderate concentrations of HFIP at either low or neutral pH efficiently induced the formation of hIAPP fibrils. In the absence of HFIP at neutral pH, hIAPP tended to form amorphous aggregates, suggesting that HFIP destabilizes a pathway leading to these aggregates and instead stabilizes the pathway to the fibrils. Here, we propose that the amyloid fibril is a unique conformation of proteins of relatively short length and peptides when they are excluded from water.

EXPERIMENTAL PROCEDURES

Materials—hIAPP peptides were purchased from the Peptide Institute, Inc (Osaka, Japan). ThT was obtained from Wako (Osaka, Japan). Buffers, salts, and solvents were obtained from Nacalai Tesque Co., Ltd (Kyoto, Japan).

Preparation of hIAPP Peptide—hIAPP contains many hydrophobic amino acid residues and so is often difficult to dissolve completely in aqueous solutions (supplemental Fig. S1*A*). Thus, we optimized the method to dissolve lyophilized hIAPP (supplemental Fig. S1*B*). First, lyophilized hIAPP was dissolved completely in 80% (v/v) HFIP containing 10 mM HCl. The CD spectrum showed a typical α-helical conformation that was stable for several days (supplemental Fig. S1*C*). Then the solution was lyophilized to remove HFIP, and the lyophilized hIAPP was dissolved in 10 mM HCl. Insoluble species were removed by ultracentrifugation. The dissolved hIAPP in 10 mM HCl (supplemental Fig. S1*D*) was immediately used for the experiments.

The formation of hIAPP fibrils was initiated by adding the stock solution to the reaction buffer. Conditions were optimized at low pH (25 μM hIAPP in 10 mM HCl at various concentrations of HFIP) and at neutral pH (25 μM hIAPP in 50 mM sodium phosphate buffer at pH 7.0 containing various concentrations of HFIP). These samples were incubated for several hours at 25 °C.

Direct Observation of Amyloid Fibrils—The TIRFM system used to observe individual amyloid fibrils was developed based on an inverted microscope (IX70, Olympus) (Tokyo, Japan) as described (37, 38, 40). The ThT molecule was excited at 442 nm by a helium-cadmium laser (IK5552R-F, Kimmon) (Tokyo, Japan), and the Nile Red molecule was excited at 532 nm by an argon laser (Spectra-Physics) (Tokyo, Japan). The laser power was 20–60 milliwatts (argon laser, 20 milliwatts; helium-cadmium laser, 40–60 milliwatts), and the observation period was 0.4–5 s (argon laser, 0.4–2 s; helium-cadmium laser, 3–5 s). The fluorescence images were filtered with a bandpass filter (helium-cadmium laser, D490/30, Omega Optical, Bratteboro, VT; argon laser, D624/40, Semrock) and visualized using a digital steel camera (DP70, Olympus). For the TIRFM observations, an aliquot (14 μl) of sample solution was immediately deposited on a quartz slide and incubated at 25 °C for a couple of hours. Final concentrations of ThT and Nile Red were 2–5 μM and 0.1–1 μM, respectively.

Assays of Fibrils—The formation of amyloid fibrils was characterized quantitatively using a fluorescent dye (ThT) (41). Five microliters of fibril solution was mixed with 1.0 ml of 5 μM ThT in 50 mM glycine-NaOH buffer (pH 8.5). The fluorescence of ThT was measured with a Hitachi F4500 spectrophotometer (Tokyo, Japan) at room temperature and averaged for three measurements. The wavelengths of excitation and emission were 445 and 485 nm, respectively. Excitation and emission slits were set to 5 and 10 nm, respectively.

CD and AFM measurements were made with a Jasco J-600 spectropolarimeter (Tokyo, Japan) and a Digital Instruments Nanoscope IIIa scanning microscope (Veeco, Tokyo, Japan), respectively, as described (13).

RESULTS

Formation of Fibrils under Acidic Conditions—In the absence of HFIP in 10 mM HCl (Fig. 1*B*), the CD spectrum, immediately after preparation of the sample, showed a fully unfolded conformation. The spectrum, after a lag time of 1 day, slowly converted to that of a β-structure (Fig. 1*B*). This conformational transition was accompanied by a slight increase in ThT fluorescence (Fig. 1*A*). The AFM measurement for the sample incubated for 5 days revealed the formation of long and straight fibrils (Fig. 1*C*). Upon addition of 10% (v/v) HFIP in 10 mM HCl, the far-UV CD spectrum showed the formation of an α-helical structure at time zero (Fig. 1*E*). The α-helical structure was converted to the β-sheet structure in 2 h. The acceleration of the reaction was also detected by ThT fluorescence (Fig. 1*D*). The AFM measurement for the sample incubated for 6 h confirmed the formation of long and straight fibrils (Fig. 1*F*). In the presence of high concentrations of HFIP (more than 20% (v/v)), hIAPP remained in an α-helical conformation, and the intensity of ThT fluorescence did not increase, even after several days of incubation (supplemental Fig. S2).

The ellipticity at 218 nm before and after the reaction and ThT fluorescence intensity after the reaction were plotted

against the concentration of HFIP (Fig. 2*A*). ThT fluorescence exhibited a maximum at 5% (v/v) HFIP. Fibrils formed before the α-helical structure was maximally stabilized at 30% (v/v) HFIP. These results indicate that, although hIAPP forms fibrils even in the absence of HFIP, a moderate concentration of HFIP accelerates the process with a maximum effect at around 5% (v/v).

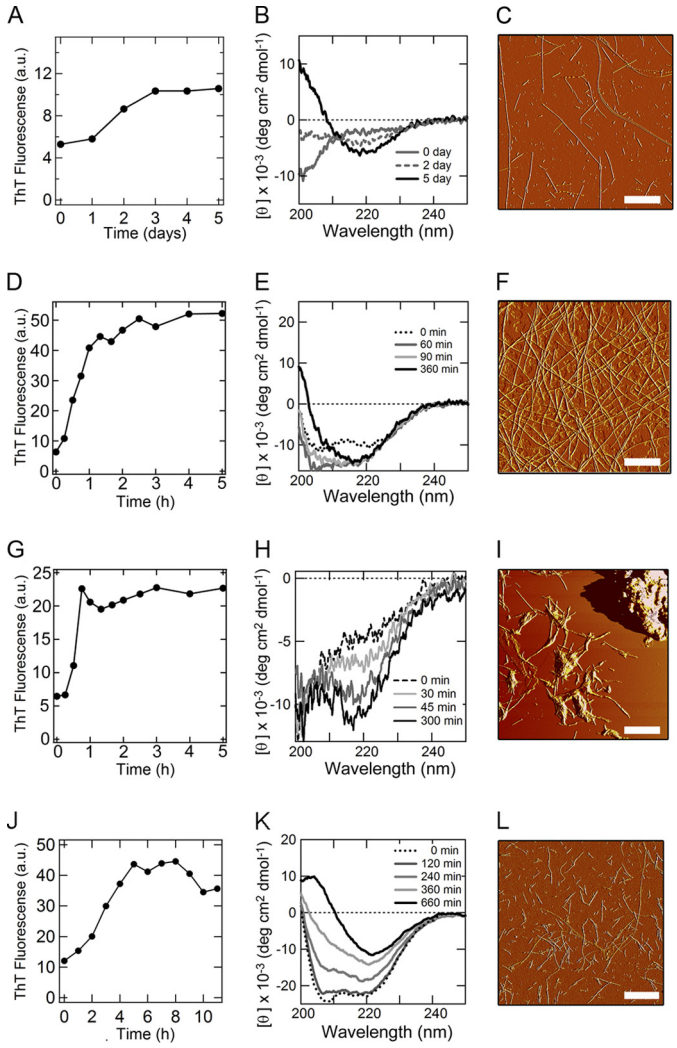

FIGURE 1. **Formation of amyloid fibrils by hIAPP monitored using the ThT-binding assay, far-UV CD, and AFM.** *A–F,* acidic conditions in 10 mM HCl in the absence (*A–C*) and presence (*D–F*) of 10% (v/v) HFIP. *G–L*, neutral conditions in the absence (*G–I*) and presence (*J–L*) of 30% (v/v) HFIP. *A, D, G,* and *J,* ThT-binding assay. *B, E, H,* and *K,* far-UV CD measurements. *C, F, I,* and *L*, AFM observations. The concentrations of the hIAPP monomers were 25 μM. The temperature for the ThT and CD measurements was 25 °C. *Scale bar* = 1 μm.

Formation of Fibrils under Neutral Conditions—We then examined the formation of fibrils of hIAPP at neutral pH in the presence of various concentrations of HFIP (Fig. 1, *G–L* and supplemental Fig. S3). Although the rate of spontaneous fibril growth in 50 mM sodium phosphate buffer at pH 7.0 without HFIP was similar to that at low pH in 10 mM HCl and 10% (v/v) HFIP, the intensity of ThT fluorescence was low (Fig. 1*G*). Additionally, CD spectra did not show a clear transition to the β-sheet structure, suggesting that hIAPP formed not only fibrils but also amorphous aggregates (Fig. 1*H*). AFM revealed that the fibrils and large aggregates coexisted (Fig. 1*I*). It is likely that hydrophobic interactions that are too strong result in the formation of amorphous aggregates as well as amyloid fibrils.

In the presence of 10–25% (v/v) HFIP, a β-sheet structure formed within 1 min, the dead time of the measurement (supplemental Fig. S3, *B–D*). In contrast, in the presence of 30% (v/v) HFIP, the CD spectrum indicated an α-helical structure that was slowly converted to a β-sheet (Fig. 1*K*). Although the fibrils formed slowly, the ThT intensity was 2-fold higher than that in the absence of HFIP (Fig. 1*J*). The AFM measurements confirmed the formation of straight fibrils without notable aggregates (Fig. 1*L*). In the presence of high concentrations of HFIP, more than 40% (v/v), hIAPP remained in the α-helical conformation, and the intensity of ThT fluorescence did not change, even after several days of incubation (supplemental Fig. S3, *F–I*).

ThT fluorescence intensity after the incubation plotted against the concentration of HFIP showed a maximum at 25% (v/v) HFIP (Fig. 2*B*), which was higher than the maximal concentration (5% (v/v) HFIP) at low pH. The CD ellipticity plot at 218 nm again indicated that the conformational transition occurs before the α-helical structure is stabilized maximally at 40% (v/v) HFIP.

Real-time Monitoring of Fibril Growth—To clarify the morphology of individual fibrils, we carried out real-time monitoring by TIRFM (36–39) under acidic and neutral conditions at 25 °C in the presence of 5 μM ThT (Fig. 3 and supplemental movies S1–S3). First, to make observations within the several hours required for stable TIRM measurements, we performed

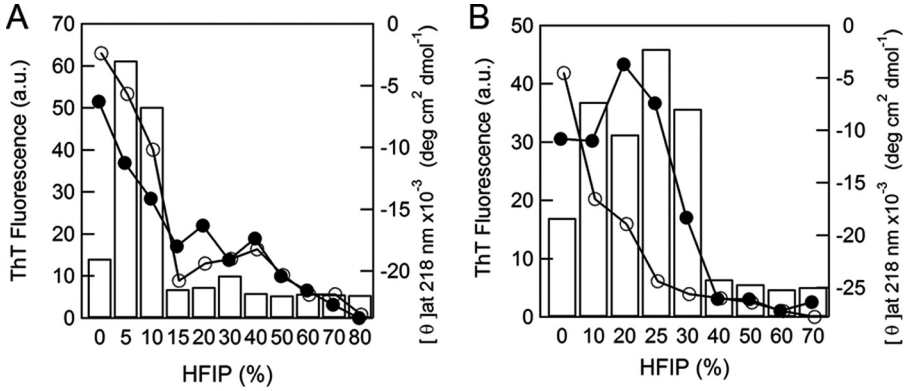

FIGURE 2. **Dependence of the formation of fibrils on the HFIP concentration.** The formation of fibrils was monitored based on ThT fluorescence (*bars*) and ellipticity at 218 nm before (○) and after (●) the reaction at low pH (*A*) and neutral pH (*B*).

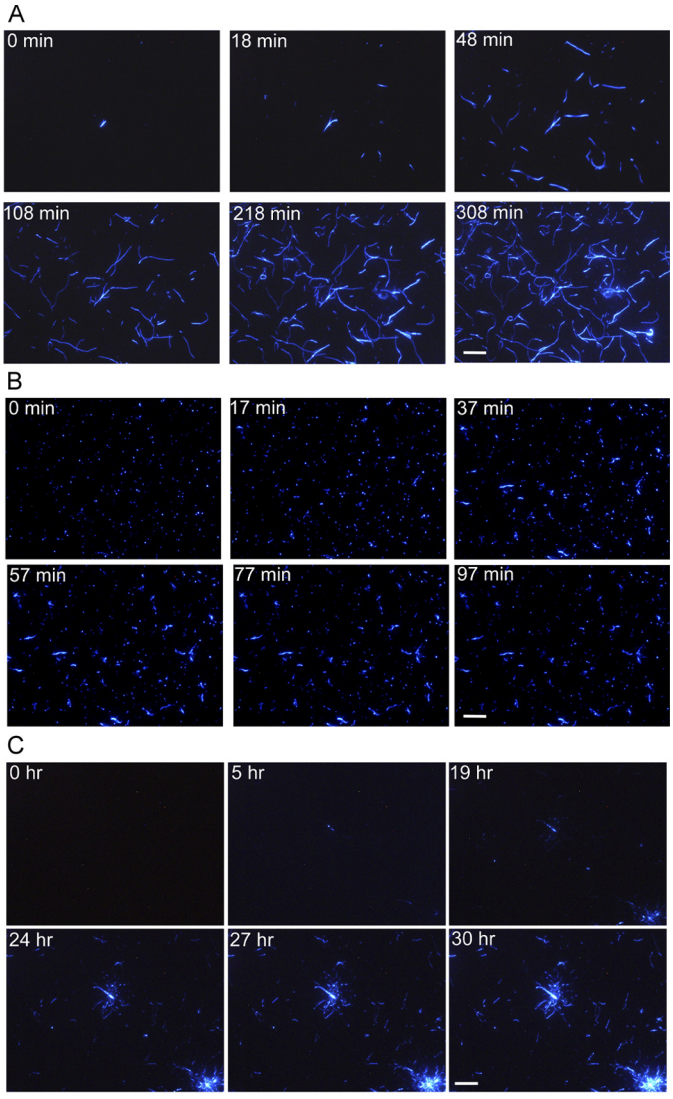

FIGURE 3. **Real-time observations of the formation of fibrils on quartz at 25 °C visualized by TIRFM.** *A*, acidic conditions in the presence of 10% (v/v) HFIP. *B* and *C*, neutral conditions in the absence (*B*) and presence (*C*) of 30% (v/v) HFIP. The concentrations of hIAPP monomers and ThT were 25 μM and 5 μM, respectively. Scale bar = 10 μm.

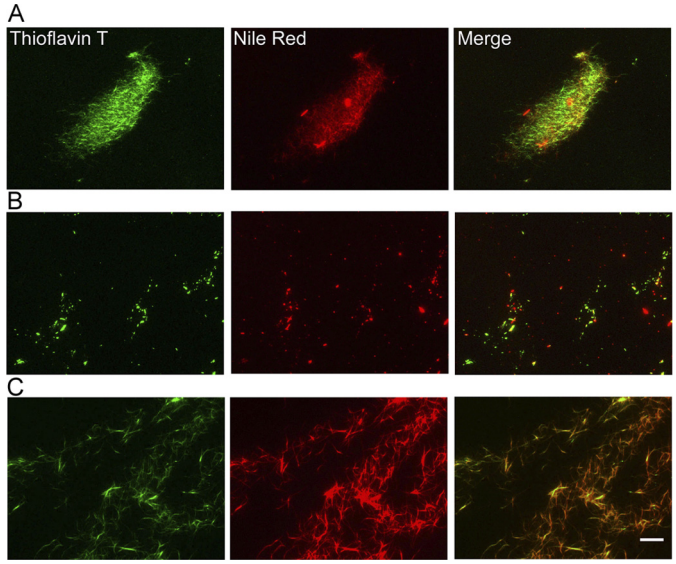

FIGURE 4. **Distinguishing amyloid fibrils from other aggregates by double-staining with ThT and Nile Red monitored by TIRFM.** *A*, hIAPP fibrils at low pH with 10% (v/v) HFIP. *B* and *C*, hIAPP fibrils at neutral pH in the absence (*B*) and presence (*C*) of 30% (v/v) HFIP. Fibrils and amorphous aggregates were visualized using ThT (*left panels*) and Nile Red (*center panels*). The *right panels* indicate merged images. The concentrations of hIAPP monomers were 12.5–25 μM. The concentrations of ThT and Nile Red were 2–5 μM and 0.1–1 μM, respectively. *Scale bar* = 10 μm.

the spontaneous fibril growth at low pH in 10 mM HCl in the presence of 10% (v/v) HFIP (Fig. 3*A* and supplemental movie S1). During the real-time monitoring, a large number of fibrils elongated from many places, indicating that the hIAPP rapidly formed nuclei for fibrillation on the quartz slide. Fibrils elongated in one direction without branching or fragmentation, reaching more than 15 μm in length. These features are consistent with those observed by AFM (Fig. 1*F*).

We then performed real-time observations of hIAPP fibril growth under neutral conditions without HFIP (Fig. 3*B* and supplemental movie S2). At time zero, numerous spots of fluorescence appeared at many places, implying that short fibrils or some kinds of aggregates reactive to ThT formed immediately after the transfer to the neutral pH buffer from 10 mM HCl. As the incubation continued, the fibrils elongated, although they were much fewer in number and shorter in length than under acidic conditions at 10% (v/v) HFIP (Fig. 3*B*).

We also observed by TIRFM the formation of fibril at neutral pH in the presence of 30% (v/v) HFIP (Fig. 3*C* and supplemental movie S3). Importantly, the fluorescence spots appeared on the quartz only after 5 h of incubation, indicating that the nucleation takes longer. After prolonged incubation for more than 1 day, a radial pattern of growth occurred at many sites. The fibrils were longer than those in the culture without HFIP, indicating that HFIP suppressed the formation of nonspecific aggregates and promoted the specific intermolecular interactions leading to the fibrillation. Nevertheless, the formation of spherulite-like structures as often observed with Aβ peptide (38, 42) suggests that the propensity for aggregation did not disappear completely even in the presence of 30% (v/v) HFIP.

Distinguishing Amyloid Fibrils from Amorphous Aggregates—We tried to distinguish amyloid fibrils from amorphous aggregates by using two dyes, the amyloid-specific ThT and Nile Red. The latter proposed to be specific to hydrophobic regions. There are reports that Nile Red binds to both nonspecific aggregates and amyloid fibrils (43, 44). Under acidic conditions with 10% (v/v) HFIP, the ThT florescence and Nile Red fluorescence overlapped (Fig. 4*A*), implying that hIAPP formed predominantly fibrils.

At neutral pH without HFIP (Fig. 4*B*), although a fraction of the ThT and Nile Red fluorescence overlapped, we detected several red spots, indicating the formation of non-amyloidogenic aggregates. As our system is unable to detect monomers or small oligomers, the red spots would represent large oligomers or nonspecific aggregates. At neutral pH in the presence of 30% (v/v) HFIP (Fig. 4*C*), the fluorescence spots of ThT and Nile Red overlapped as under the acidic conditions, suggesting that 30% (v/v) HFIP suppressed the formation of amorphous aggregates, promoting the formation of fibrils.

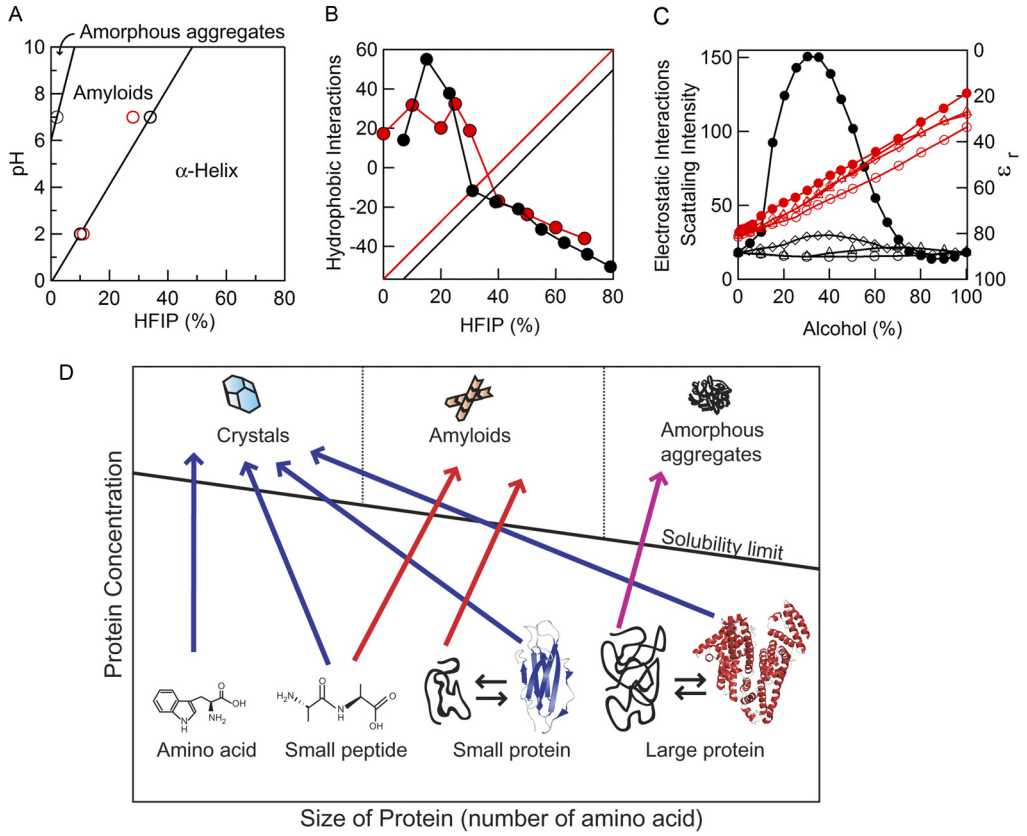

FIGURE 5. **Phase-diagrams of the formation of fibrils.** *A*, phase diagram of the pH and HFIP concentration-dependent formation of hIAPP fibrils. The boundaries of the phases were determined from the midpoint of the HFIP-dependent conformational transition monitored using ThT (○) and CD (*red circles*). *B*, contribution of hydrophobic (*circles*, *left axis*) and polar plus charge (*linear lines*, *right axis*) interactions to the hIAPP fibrils under acidic (*red*) and neutral (*black*) conditions. Polar plus charge interactions were assumed to increase linearly with an increase in the HFIP concentration. Then the linear contribution was subtracted from the ThT intensities shown in Fig. 2 to make a similar pattern of hydrophobic contributions at acidic and neutral conditions. *C*, concentration-dependent clustering of alcohols monitored by small angle x-ray scattering (*black symbols*, *left axis*) and concentration-dependent decreases in the dielectric constant of alcohols (*red symbols*, *right axis*). Although the scattering intensity represents the strength of hydrophobic interactions, the dielectric constant represents that of electrostatic interactions. Methanol (○), ethanol (△), TFE (◇) and HFIP (●). Data are from Hong *et al.* (26) *D*, general phase diagram of the length- and concentration-dependent conformational transition of peptides and proteins. Native structures of the small and large proteins represent those of β_2-microglobulin (PDB code 2D4F) and human serum albumin (PDB code 1AO6), respectively.

Detection of Oligomeric Species by Analytical Ultracentrifugation—We examined the oligomeric state of hIAPP in the early stage of fibril formation using analytical ultracentrifugation. Sedimentation velocities at 0 and 10% (v/v) HFIP under acidic conditions were monitored (supplemental Fig. S4).

Significant fractions in the absence of HFIP precipitated with the sedimentation coefficient ($s_{20,w}$) values of 0.8–1.0 S. The $s_{20,w}$ values increased to 1.0–2.0 S in the presence of 10% (v/v) HFIP, indicating the formation of larger species. On the other hand, the values of $s_{20,w}$ for the preformed fibrils were 60–70 S, consistent with our previous paper (45). We further estimated the molecular weight of these oligomeric species using $s_{20,w}$ distributions, frictional ratios, and partial specific volumes with the UltraScan software to be 6000 – 8000 (dimer) in the absence of HFIP and 10,000–20,000 (dimer-pentamer) in the presence of 10% (v/v) HFIP (supplemental Fig. S4). The results confirmed the formation of oligomeric species in the early stage of fibril formation.

DISCUSSION

Phase Diagram of HFIP and pH-dependent Conformational Transitions—The HFIP-dependent formation of fibrils by hIAPP under acidic and neutral conditions can be summarized in a phase diagram (Fig. 5*A*). The phase boundaries were determined on the basis of transitions monitored using ThT fluorescence and ellipticity at 218 nm. Fibrillation was promoted by moderate concentrations of HFIP under both sets of conditions, although the optimal concentration differed between the two. At low pH, addition of HFIP directly accelerated the formation of fibrils from the unfolded hIAPP. At neutral pH, hIAPP tended to form amorphous aggregates in the absence of HFIP, and fibrils were stabilized by the addition of HFIP. The optimal HFIP concentration for the formation of fibrils was higher at neutral pH (25% (v/v)), than at low pH (5% (v/v)). For both conditions, a further increase in the HFIP concentration caused the fibrils to dissolve completely, thus stabilizing the α-helical structure.

hIAPP has four titratable groups: the α-amino group and ϵ-amino group of Lys-1, the guanidyl group of Arg-11, and the imidazole group of His-18, with intrinsic pK_a values of 7.0, 9.0, 12<, and 7, respectively. While all of these titratable groups are positively charged at around pH 2, the α-amino group and imidazole group of His-18 are partly deprotonated at pH 7, although the extent of deprotonation is unknown. This difference produces the slightly higher net charge of hIAPP at acidic

pH than at neutral pH, creating the stronger charge repulsion at acidic pH and thus reducing the propensity to form amorphous aggregates.

The Role of Helical Intermediates—Today, a number of experimental evidence argue that the formation of an α-helical intermediate is important for amyloid formation by hIAPP (12, 34, 35). In the presence of 10% (v/v) HFIP under acidic conditions, the far-UV CD spectrum showed the formation of an α-helical structure at time zero (Fig. 1*E*). On the other hand, in the absence of HFIP, the helical propensity of hIAPP was minimal. It looks like the fibril formation is correlated with the formation of an α-helical structure, although too high a concentration of HFIP adversely suppresses the fibril formation by stabilizing the monomeric α-helical structure.

We examined the oligomeric state under different concentrations of HFIP with analytical centrifugation. Sedimentation velocity experiments showed the formation of oligomeric spices (dimer-pentamer) in 10% (v/v) HFIP (supplemental Fig. S4). Oligomeric species were formed less extensively in the absence of HFIP where hIAPP does not form an α-helical structure. Thus, the formation of oligomeric species is also correlated with the formation of fibrils. Although it took a couple of days, hIAPP finally formed fibrils even in the absence of HFIP where the helical propensity is minimal. This implies that the formation of oligomers or nonspecific aggregates is more important than the α-helical conformation for the formation of fibrils and that the accumulation of an α-helical structure as observed in 10% (v/v) HFIP represents the conformational preference of hIAPP under the conditions chosen. Further studies are necessary to clarify the role of α-helical intermediates.

Underlying Forces Producing the Bell-shaped Dependence—The bell-shaped profiles of fibril formation (Fig. 2) suggest that the conformation of hIAPP is determined by the opposing forces of fibril formation and degradation. Considering the general effects of alcohols on proteins and peptides, these forces are related to hydrophobic and electrostatic interactions. Usually hydrophobic interactions are expected to decrease with an increase in the concentration of hydrophobic alcohols, although the situation is more complicated for HFIP and TFE (see below) (25, 26). In contrast, electrostatic interactions, including polar interactions and charge-charge interactions, increase with an increase in the concentration of HFIP.

We attempted to analyze the observed bell-shaped dependence (Fig. 2) as a sum of these opposing contributions. We assumed that a total of electrostatic interactions increase linearly with an increase in the concentration of HFIP. This assumption is based on the finding that the dielectric constant of the solvent decreases linearly with an increase in the concentration of HFIP (26) (Fig. 5*C*). Similar linear decreases in the dielectric constant are observed with various alcohols, including TFE, methanol, and ethanol (26). Assuming a linear dependence of electrostatic interactions, for the optimum formation of fibrils the hydrophobic interaction should also exhibit an optimum (Fig. 5*B*).

Although the idea of optimum for hydrophobic interactions seems strange at first, it should be noted that HFIP forms micelle-like dynamic clusters at around 30% (v/v) (25, 26) (Fig. 5*C*). Dynamic clusters of HFIP are formed by hydrophobic interactions, enhancing the hydrophobic interactions between solutes. This leads to various effects, such as an increased propensity to form an α-helix or an aggregate or greater amyloidogenicity, depending on the peptides and conditions. In the case of amyloidogenicity, the combined effects of enhancing both hydrophobic and polar interactions may explain why fibrils are formed efficiently at a moderate concentration of HFIP. A similar dynamic clustering occurs with TFE, although to a lesser extent than with HFIP (Fig. 5*C*). It is important to note that the alcohol-induced aggregation and fibrillation occur before the optimal concentration for clustering, suggesting that the interactions with partially clustered hydrophobic cosolvents increase the overall hydrophobicity of the peptides, leading to the association and aggregation. In contrast, the formation of such clusters is not significant for other small alcohols like methanol and ethanol, even if marginal clusters are formed (Fig. 5*C*). This may explain why HFIP and TFE are particularly useful for forming the fibrils. The interpretation of the effects of HFIP on peptides probably applies to SDS, another cosolvent promoting the formation of fibrils at concentrations below its CMC (13).

Then what is the difference between amyloid fibrils and amorphous aggregates? At neutral pH, hydrophobic interactions may be too strong compared with polar and electrostatic interactions, causing hIAPP to associate without a hydrogen bond network. To make the fibrils, a higher concentration of HFIP (25%) was required, by which hydrophobic interactions are slightly weakened and polar interactions are strengthened (Fig. 5*B*).

The arguments made above suggest that amyloid fibrils and amorphous aggregates are different forms of protein precipitates produced by the exclusion of polypeptides from water-alcohol mixtures. If this is the case, it is likely that the solubility of hIAPP decreases notably at moderate concentrations of HFIP, TFE, or SDS coupled with the formation of fibrils. Although the solubility of polypeptides in HFIP or TFE has not been studied, for many systems the solubility of proteins and peptides decreases markedly slightly below the CMC of SDS, conditions under which the development of fibrils is also promoted (26).

Dependence of Fibril Formation on Peptide Length—With hIAPP, we suggested that the balance between hydrophobic interactions and polar and electrostatic interactions determines the solubility of the monomeric polypeptide, thus determining the conformation of peptides from amorphous aggregates, fibrils, and the monomeric helical conformation. If fibril formation is determined by the solubility of polypeptides, another important factor is the length of peptides. It is obvious that fibrillar deposition is common among shorter peptides but rare for proteins of more than 200 amino acids. As far as we know, the longest protein in which an entire region forms fibrils is apomyoglobin (16, 17). Moreover, there are numerous examples of fragments derived from larger proteins forming fibrils (19). These fibrils are often more ordered, *i.e.* rigid and straight, than those of their original proteins. Very short amyloidogenic peptides form microcrystals useful for x-ray diffraction analysis (11, 20, 21). From all this evidence one can construct a general phase diagram of protein conformation dependent on the

length of the polypeptides (Fig. 5*D*). The diagram is a simplified one of the transition between a solution and a solid and so does not include intermediates such as oligomeric aggregates and soluble fibrils.

One can assume four types of phase transition from a solution to a solid phase. 1) Small molecules with low conformational flexibility: When the concentration of an amino acid exceeds limit of solubility, precipitation produces single crystals or a monocrystalline solid. Here, the phase transition from a solution to a solid is equal to the formation of crystals. If the length increases to several amino acid residues, single crystals may still form. Amyloid monocrystals may represent such a case, in which tightly packed steric zippers are found (11, 20, 21). 2) Large molecules with low conformational flexibility: Even a large protein can form single crystals useful for x-ray crystallography as long as its flexibility is fixed. 3) Large molecules with high flexibility: However, once denatured larger proteins cannot form crystals because of heterologous intermolecular interactions. Thus, a unique conformation is essential for single crystals to form. 4) Peptides of moderate size: When peptides become longer, the longitudinal interactions between them to form the cross-β structure remain, whereas the lateral interactions between β-sheets to form tightly packed amyloid crystals become disturbed, producing ordered amyloid fibrils. However, with an increase in length, a variety of alternative interactions eventually prevent the formation of cross-β sheets, resulting in amorphous aggregates.

This length-dependent transition from three-dimensional single crystals to amorphous aggregates with intermediate amyloid structures may be a unique property of polypeptide chains that can form both hydrophobic interactions and hydrogen bonds (Fig. 5*D*). The boundaries between the three phases depend on the sequence and amino acid composition. Sequences with a low propensity to form a secondary structure like Pro and Gly prevent or narrow amyloidogenic regions (46). So far, the amyloidogenicity of proteins and peptides has been compared at the same concentrations. The idea that the amyloid conformation is one type of structure that unfolded proteins assume when they are excluded from interactions with water suggests that even peptides of low amyloidogenicity can form amyloid fibrils when their concentration exceeds the solubility limit.

CONCLUSION

In conclusion, the formation of fibrils by hIAPP in the presence of various concentrations of HFIP suggests that amyloid fibrils are one type of protein precipitate formed upon exclusion from an aqueous environment. Amyloid fibrils are distinct from amorphous aggregates in terms of the organized formation of hydrophobic interactions and hydrogen bonds, which is promoted in the presence of moderate concentrations of HFIP. The effects of moderate concentrations of HFIP or SDS may mimic the membrane environment, accelerating the formation of fibrils. We also suggest that the length of the polypeptide chain is critical in determining the morphology of the precipitates of polypeptides, from single crystals to amyloid fibrils and amorphous aggregates.

Acknowledgments—We thank Drs. Tetsuichi Wazawa (Tohoku University) and Tadato Ban (University of Fukui) for support with the TIRFM system. We also thank Miyo Sakai for help with the analytical ultracentrifugation.

REFERENCES

1. Sipe, J. D. (1994) *Crit. Rev. Clin. Lab. Sci.* **31,** 325–354
2. Dobson, C. M. (2003) *Nature* **426,** 884–890
3. Selkoe, D. J. (2004) *Nat. Cell Biol.* **6,** 1054–1061
4. Yamamoto, S., and Gejyo, F. (2005) *Biochim. Biophys. Acta* **1753,** 4–10
5. Chiti, F., and Dobson, C. M. (2006) *Annu. Rev. Biochem.* **75,** 333–366
6. Fowler, D. M., Koulov, A. V., Balch, W. E., and Kelly, J. W. (2007) *Trends Biochem. Sci.* **32,** 217–224
7. Maji, S. K., Perrin, M. H., Sawaya, M. R., Jessberger, S., Vadodaria, K., Rissman, R. A., Singru, P. S., Nilsson, K. P., Simon, R., Schubert, D., Eisenberg, D., Rivier, J., Sawchenko, P., Vale, W., and Riek, R. (2009) *Science* **325,** 328–332
8. Kelly, J. W. (1998) *Curr. Opin. Struct. Biol.* **8,** 101–106
9. Khurana, R., Gillespie, J. R., Talapatra, A., Minert, L. J., Ionescu-Zanetti, C., Millett, I., and Fink, A. L. (2001) *Biochemistry* **40,** 3525–3535
10. Raimondi, S., Guglielmi, F., Giorgetti, S., Gaetano, S. D., Arciello, A., Monti, D. M., Relini, A., Nichino, D., Doglia, S. M., Natalello, A., Pucci, P., Mangione, P., Obici, L., Merlini, G., Stoppini, M., Robustelli, P., Tartaglia, G. G., Vendruscolo, M., Dobson, C. M., Piccoli, R., and Bellotti, V. (2011) *J. Mol. Biol.* **407,** 465–476
11. Nelson, R., and Eisenberg, D. (2006) *Adv. Protein Chem.* **73,** 235–282
12. Anderson, V. L., Ramlall, T. F., Rospigliosi, C. C., Webb, W. W., and Eliezer, D. (2010) *Proc. Natl. Acad. Sci. U.S.A.* **107,** 18850–18855
13. Yamaguchi, K., Naiki, H., and Goto, Y. (2006) *J. Mol. Biol.* **363,** 279–288
14. Ahmad, M. F., Ramakrishna, T., Raman, B., and Rao, Ch. M. (2006) *J. Mol. Biol.* **364,** 1061–1072
15. Giehm, L., Oliveira, C. L., Christiansen, G., Pedersen, J. S., and Otzen, D. E. (2010) *J. Mol. Biol.* **401,** 115–133
16. Fändrich, M., Fletcher, M. A., and Dobson, C. M. (2001) *Nature* **410,** 165–166
17. Fändrich, M., Forge, V., Buder, K., Kittler, M., Dobson, C. M., and Diekmann, S. (2003) *Proc. Natl. Acad. Sci. U.S.A.* **100,** 15463–15468
18. Kozhukh, G. V., Hagihara, Y., Kawakami, T., Hasegawa, K., Naiki, H., and Goto, Y. (2002) *J. Biol. Chem.* **277,** 1310–1315
19. Häggqvist, B., Näslund, J., Sletten, K., Westermark, G. T., Mucchiano, G., Tjernberg, L. O., Nordstedt, C., Engström, U., and Westermark, P. (1999) *Proc. Natl. Acad. Sci. U.S.A.* **96,** 8669–8674
20. Nelson, R., Sawaya, M. R., Balbirnie, M., Madsen, A.Ø., Riekel, C., Grothe, R., and Eisenberg, D. (2005) *Nature* **435,** 773–778
21. Sawaya, M. R., Sambashivan, S., Nelson, R., Ivanova, M. I., Sievers, S. A., Apostol, M. I., Thompson, M. J., Balbirnie, M., Wiltzius, J. J., McFarlane, H. T., Madsen, A. Ø., Riekel, C., and Eisenberg, D. (2007) *Nature* **447,** 453–457
22. Tartaglia, G. G., Pechmann, S., Dobson, C. M., and Vendruscolo, M. (2009) *J. Mol. Biol.* **388,** 381–389
23. Pechmann, S., and Vendruscolo, M. (2010) *Mol. Biosyst.* **6,** 2490–2497
24. Buck, M. (1998) *Q. Rev. Biophys.* **31,** 297–355
25. Hirota, N., Mizuno, K., and Goto, Y. (1998) *J. Mol. Biol.* **275,** 365–378
26. Hong, D. P., Hoshino, M., Kuboi, R., and Goto, Y. (1999) *J. Am. Chem. Soc.* **121,** 8427–8433
27. Clark, A., Cooper, G. J., Lewis, C. E., Morris, J. F., Willis, A. C., Reid, K. B., and Turner, R. C. (1987) *Lancet* **2,** 231–234
28. Cooper, G. J., Willis, A. C., Clark, A., Turner, R. C., Sim, R. B., and Reid, K. B. (1987) *Proc. Natl. Acad. Sci. U.S.A.* **84,** 8628–8632
29. Westermark, P., Wernstedt, C., Wilander, E., Hayden, D. W., O'Brien, T. D., and Johnson, K. H. (1987) *Proc. Natl. Acad. Sci. U.S.A.* **84,** 3881–3885
30. Kahn, S. E., Andrikopoulos, S., and Verchere, C. B. (1999) *Diabetes* **48,** 241–253
31. Marzban, L., Park, K., and Verchere, C. B. (2003) *Exp. Gerontol.* **38,** 347–351

32. Hull, R. L., Westermark, G. T., Westermark, P., and Kahn, S. E. (2004) *J. Clin. Endocrinol. Metab.* **89,** 3629–3643
33. Engel, M. F., Khemtémourian, L., Kleijer, C. C., Meeldijk, H. J., Jacobs, J., Verkleij, A. J., de Kruijff, B., Killian, J. A., and Höppener, J. W. (2008) *Proc. Natl. Acad. Sci. U.S.A.* **105,** 6033–6038
34. Hebda, J. A., and Miranker, A. D. (2009) *Annu. Rev. Biophys.* **38,** 125–152
35. Abedini, A., and Raleigh, D. P. (2009) *Phys. Biol.* **6,** 15005
36. Ban, T., Hamada, D., Hasegawa, K., Naiki, H., and Goto, Y. (2003) *J. Biol. Chem.* **278,** 16462–16465
37. Ban, T., Hoshino, M., Takahashi, S., Hamada, D., Hasegawa, K., Naiki, H., and Goto, Y. (2004) *J. Mol. Biol.* **344,** 757–767
38. Ban, T., Morigaki, K., Yagi, H., Kawasaki, T., Kobayashi, A., Yuba, S., Naiki, H., and Goto, Y. (2006) *J. Biol. Chem.* **281,** 33677–33683
39. Ban, T., Yamaguchi, K., and Goto, Y. (2006) *Acc. Chem. Res.* **39,** 663–670
40. Yagi, H., Ozawa, D., Sakurai, K., Kawakami, T., Kuyama, H., Nishimura, O., Shimanouchi, T., Kuboi, R., Naiki, H., and Goto, Y. (2010) *J. Biol. Chem.* **285,** 19660–19667
41. Naiki, H., Hashimoto, N., Suzuki, S., Kimura, H., Nakakuki, K., and Gejyo, F. (1997) *Amyloid.* **4,** 223–232
42. Yagi, H., Ban, T., Morigaki, K., Naiki, H., and Goto, Y. (2007) *Biochemistry* **46,** 15009–15017
43. Demeule, B., Gurny, R., and Arvinte, T. (2007) *Int. J. Pharm.* **329,** 37–45
44. Mishra, R., Sörgjerd, K., Nyström, S., Nordigården, A., Yu, Y. C., and Hammarström, P. (2007) *J. Mol. Biol.* **366,** 1029–1044
45. Chatani, E., Lee, Y. H., Yagi, H., Yoshimura, Y., Naiki, H., and Goto, Y. (2009) *Proc. Natl. Acad. Sci. U.S.A.* **106,** 11119–11124
46. Parrini, C., Taddei, N., Ramazzotti, M., Degl'Innocenti, D., Ramponi, G., Dobson, C. M., and Chiti, F. (2005) *Structure* **13,** 1143–1151

Hexafluoroisopropanol Induces Amyloid Fibrils of Islet Amyloid Polypeptide by Enhancing Both Hydrophobic and Electrostatic Interactions

Kotaro Yanagi, Mizue Ashizaki, Hisashi Yagi, Kazumasa Sakurai, Young-Ho Lee and Yuji Goto

J. Biol. Chem. 2011, 286:23959-23966.
doi: 10.1074/jbc.M111.226688 originally published online May 12, 2011

Supplemental Figures

Hexafluoroisopropanol induces amyloid fibrils of islet amyloid polypeptide by enhancing both hydrophobic and electrostatic interactions

Kotaro Yanagi, Mizue Ashizaki, Hisashi Yagi, Kazumasa Sakurai, Young-Ho Lee and Yuji Goto

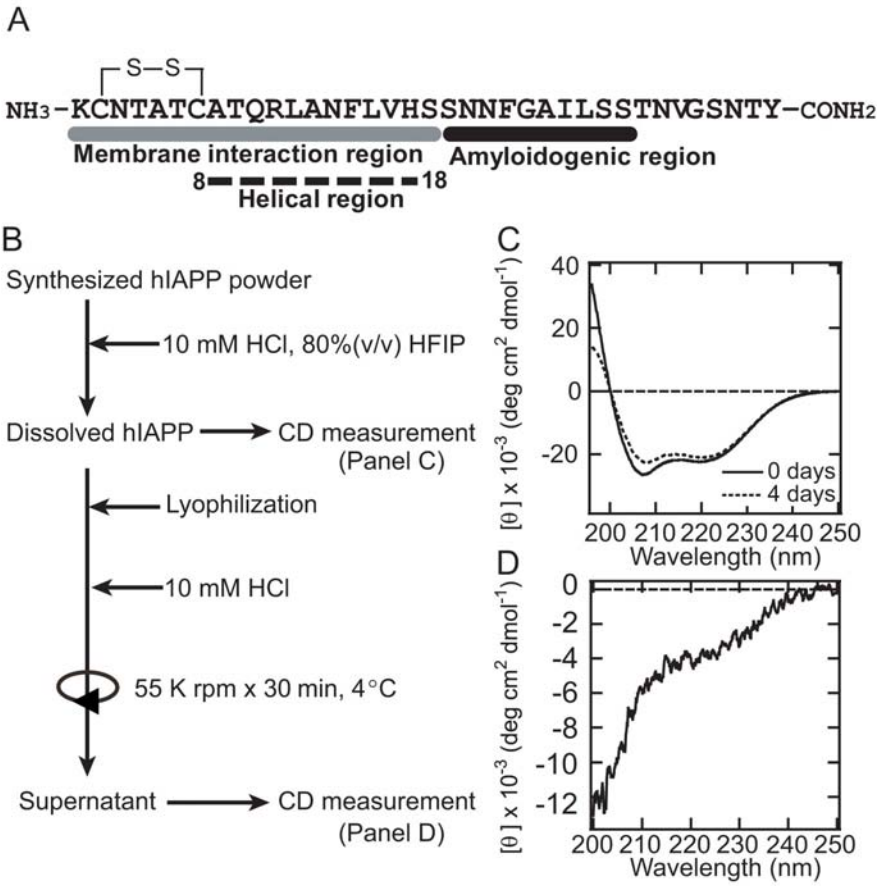

Supplemental Fig. S1. The sample preparation of hIAPP. (*A*) Amino acid sequence and structural properties of hIAPP. (*B*) Schematic diagram of the method used. (*C*) Far-UV CD spectra of hIAPP in 10 mM HCl with 80% (v/v) HFIP (solid line: 0 days, dashed line: 4 days). (*D*) Far-UV CD spectrum of hIAPP in 10 mM HCl after ultracentrifugation.

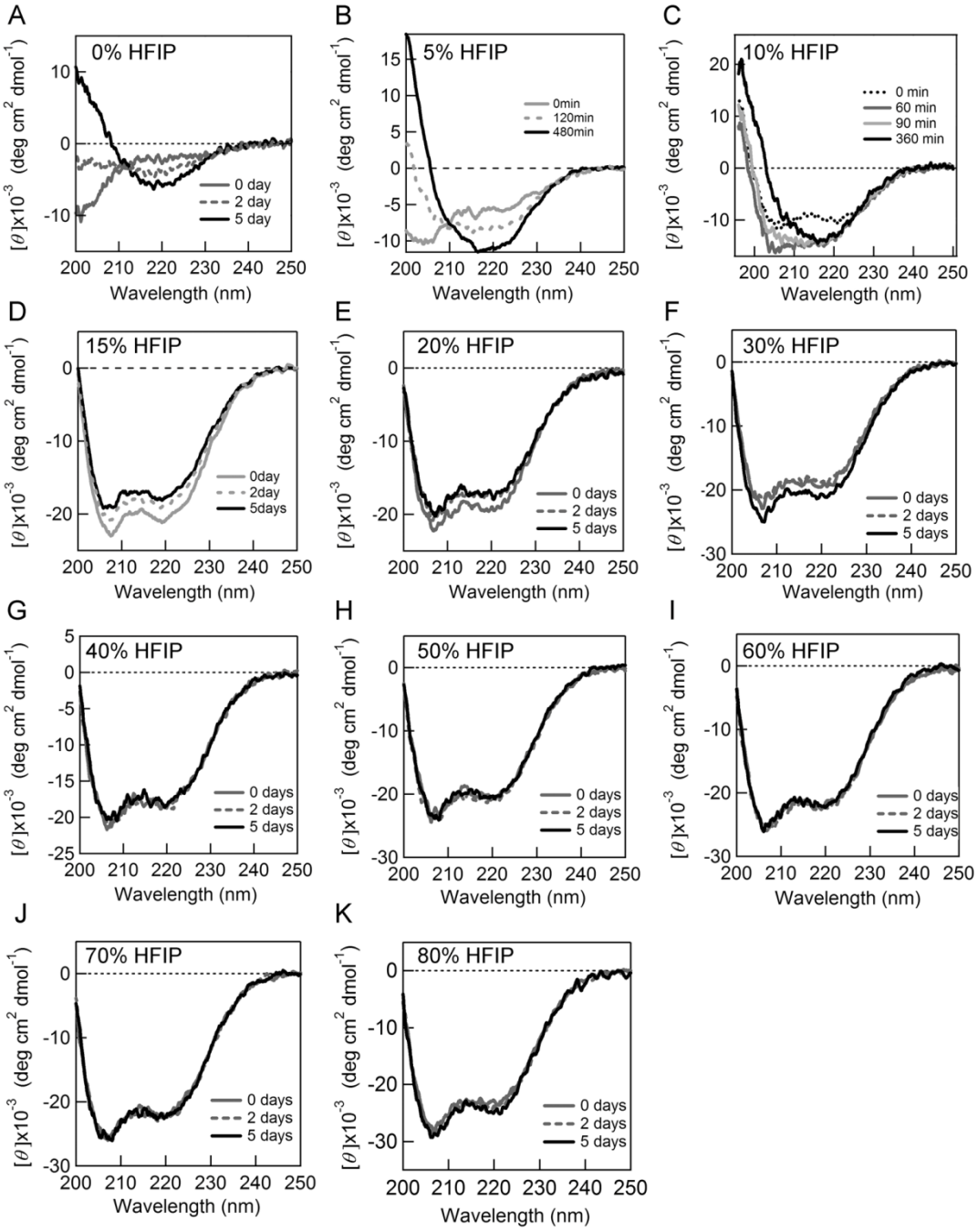

Supplemental Fig. S2. Time-dependent changes of the far-UV CD spectra of 25 μM hIAPP at various concentrations of HFIP in 10 mM HCl at 25°C.

Yanagi et.al., Supplemental Fig. S2

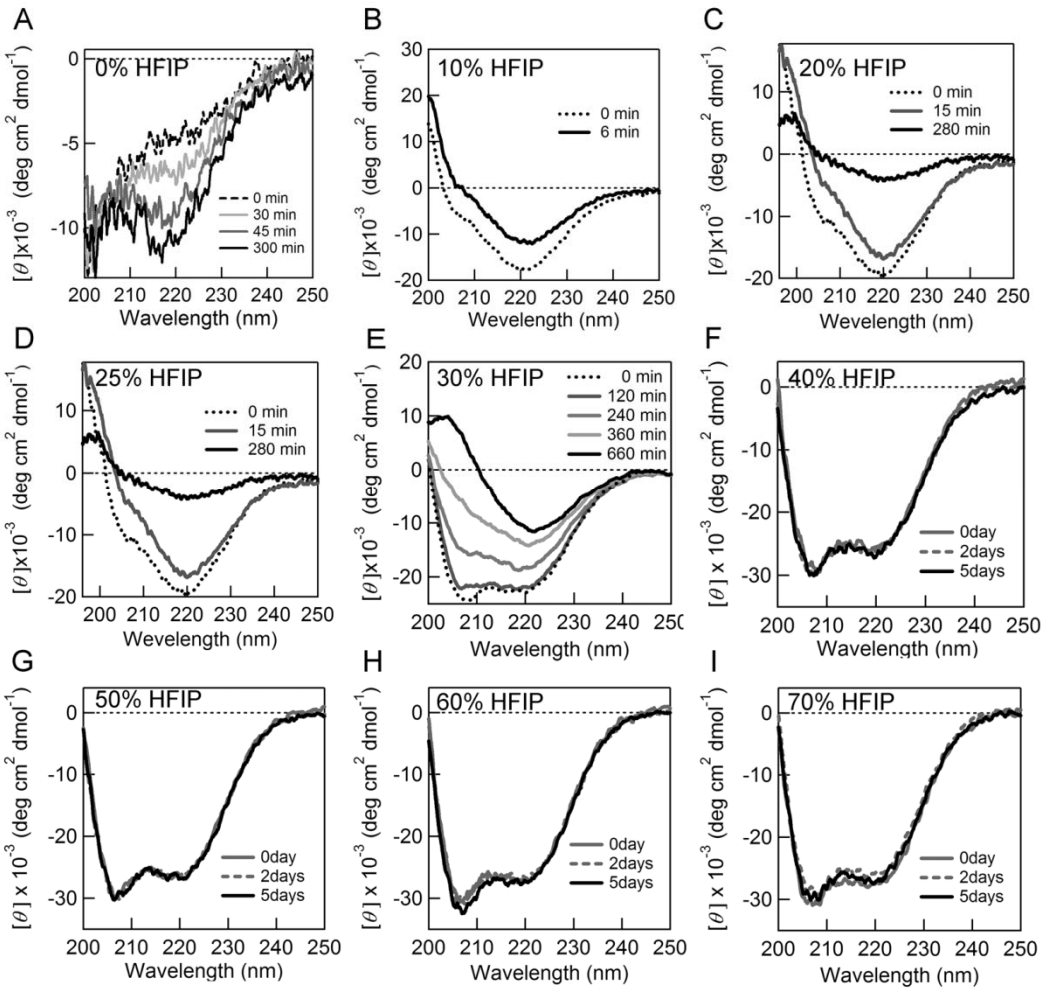

Supplemental Fig. S3. Time-dependent changes of the far-UV CD spectra of 25 μM hIAPP at various concentrations of HFIP in 10 mM sodium phosphate buffer at pH 7.0 and at 25°C.

Yanagi et.al., Supplemental Fig. S3

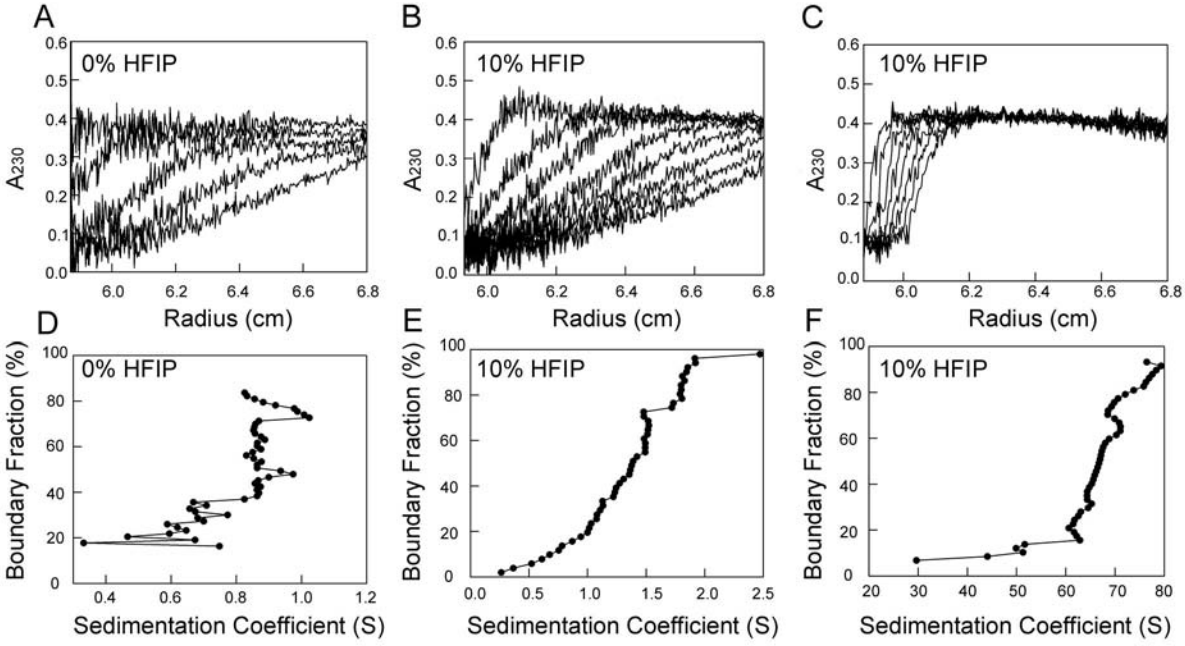

Supplemental Fig. S4. Sedimentation velocity experiments of 25 μM hIAPP of various conformations in the absence and presence of 10% (v/v) HFIP in 10 mM HCl and 25°C. (*A*-*C*) Sedimentation boundary profiles of hIAPP oligomers in the absence (*A*) and presence (*B*) of 10% (v/v) HFIP and preformed hIAPP fibrils in the presence of 10% (v/v) HFIP (*C*). Centrifugation was performed at 55,000 rpm (230,000 × *g*) (*A*-*B*) and 6,000 rpm (2,700 × *g*) (*C*) by monitoring the absorbance at 230 nm at intervals of 200 min (*A*), 100 min (*B*), and 25 min (*C*), respectively. Integral distribution plots of the sedimentation coefficient ($s_{20,w}$), corrected for the viscosity and density of the solvent using that of water at 20°C, were shown in the absence (*D*) and presence (*E*, *F*) of 10% (v/v) HFIP. Sedimentation velocity experiments were performed using a Beckman-Coulter Optima XL-A analytical ultracentrifuge (Fullerton, CA) after precentrifugation at 3,000 rpm (700 × *g*) for 5 min. The experimental sedimentation coefficients were corrected to $s_{20,w}$, the sedimentation coefficient expressed in terms of the standard solvent of water at 20°C, with the van Holde-Weischet method in the software UltraScan 8.0 (www.ultrascan.uthscsa.edu). Molecular weights of oligomeric species were estimated using $s_{20,w}$ distributions, frictional ratios, and partial specific volumes with the UltraScan software.

Supplemental movies

Supplemental Movie S1: Real-time observation of fibril growth under acidic conditions in the presence of 10% (v/v) HFIP and 5 μM ThT at 25 °C.

Supplemental Movie S2: Real-time observation of fibril growth under neutral conditions (pH 7.0) in the presence of 5 μM ThT at 25 °C.

Supplemental Movie S3: Real-time observation of fibril growth under neutral conditions in the presence of 30% (v/v) HFIP and 5 μM ThT at 25 °C.